

Helium atmospheric pressure plasma jets interacting with wet cells: delivery of electric fields

Seth A Norberg^{1,4}, Eric Johnsen¹ and Mark J Kushner^{2,3}

¹ University of Michigan, Department of Mechanical Engineering, 2350 Hayward Street, Ann Arbor, MI 48109-2125, USA

² University of Michigan, Department of Electrical Engineering and Computer Science, 1301 Beal Avenue, Ann Arbor, MI 48109-2122, USA

E-mail: norbergs@umich.edu, ejohnsen@umich.edu and mjkush@umich.edu

Received 28 January 2016, revised 10 March 2016

Accepted for publication 16 March 2016

Published 5 April 2016



Abstract

The use of atmospheric pressure plasma jets (APPJs) in plasma medicine have produced encouraging results in wound treatment, surface sterilization, deactivation of bacteria, and treatment of cancer cells. It is known that many of the reactive oxygen and nitrogen species produced by the APPJ are critical to these processes. Other key components to treatment include the ion and photon fluxes, and the electric fields produced in cells by the ionization wave of the APPJ striking in the vicinity of the cells. These relationships are often complicated by the cells being covered by a thin liquid layer—wet cells. In this paper, results from a computational investigation of the interaction of APPJs with tissue beneath a liquid layer are discussed. The emphasis of this study is the delivery of electric fields by an APPJ sustained in He/O₂ = 99.8/0.2 flowing into humid air to cells lying beneath water with thickness of 200 μm. The water layer represents the biological fluid typically covering tissue during treatment. Three voltages were analyzed—two that produce a plasma effluent that touches the surface of the water layer and one that does not touch. The effect of the liquid layer thickness, 50 μm to 1 mm, was also examined. Comparisons were made of the predicted intracellular electric fields to those thresholds used in the field of bioelectronics.

Keywords: plasma medicine, plasma liquid interactions, atmospheric pressure plasma, plasma jets, electroporation, electric fields and cells, modeling

(Some figures may appear in colour only in the online journal)

1. Introduction

Atmospheric pressure plasma jets (APPJs) are the subject of much interest resulting from their use in biotechnology [1]. The active species or activated systems produced by APPJs have been shown to deactivate bacteria [2], sterilize surfaces [3], heal wounds [4] and selectively eradicate cancer cells *in vitro* and reduce tumor size *in vivo* [5, 6]. The mechanisms responsible for these successful outcomes are still poorly

understood. One set of mechanisms relies on the reactive oxygen and nitrogen species (RONS) produced by APPJs which contribute to the treatment of the biological surface through signaling mechanisms, oxygenation, and providing activation energy by the delivery of charged species and photons [1]. Another path to activation is aqueous ion species produced by APPJs in contact with cell-covering-liquids that in turn trigger intracellular responses [7, 8].

The experimental characterization of APPJs in the context of treating biological materials has produced the following general picture of their operation [9–12]. A rare gas, perhaps seeded with a small fraction of a reactive gas, is flowed through a tube

³ Author to whom correspondence should be addressed.

⁴ Present address: United States Military Academy, Department of Civil and Mechanical Engineering, West Point, NY 10996, USA.

into room air. A pulsed or sinusoidal voltage applied to electrodes in or around the tube initiates a discharge in the rare gas. Typically at most one electrode is in the tube and so the discharge is akin to a dielectric barrier device. An ionization wave propagates from within the tube through the rare-gas dominated plume outside the tube, extending the applied voltage and large electric field to the head of the ionization wave [13, 14]. Reactive species are produced by electron impact with both the seeded molecular gas in the flow and with the ambient gases diffusing into the rare-gas plume. The ionization wave will terminate when the mole fraction of ambient gases in the rare gas plume exceeds a critical value while also being sensitive to the configuration of the electrodes [15]. If the ionization wave reaches the surface being treated, this is termed a touching plasma jet, which can produce charging of the surface [16, 17]. Otherwise, the APPJ is not-touching. In addition to the neutral radicals produced by the APPJ which are entrained in the flow, UV and VUV radiation can also be incident onto the surface.

When treating cells, APPJs also produce electric fields which can potentially affect the electric potential of the plasma membrane as well as the mitochondria in the cytoplasm. For example, recent work has demonstrated a reduced mitochondria membrane potential, indicating cytochrome *c* release (an early indicator of apoptosis), by using a combined treatment of soft air plasma and 2-deoxy-D-glucose *in vitro* [18]. APPJs are being investigated as a method for more efficient and less invasive gene transfection. High transfection efficiency was reported at two distinct points during the treatment time. The first peak was attributed to stimulation by electric fields and the second resulted from the cumulative effects of oxidative stress [19]. The computational results discussed in this paper address the delivery of such electric fields to cells by APPJs resulting from propagating ionization waves which strike the liquid covering cells. Recent experiments by Roberts *et al* have shown that such plasma-jet delivered electric fields can penetrate many mm deep into mammalian tissue [20, 21].

The effects of the electric field of the discharge as well as the local electric field produced by charging of surfaces on cells are addressed by the field of bioelectronics [22–24]. The amplitude and duration of the voltage pulse applied to the cell can produce significantly different outcomes [16]. At low electric fields (a few kV cm^{-1}), but long pulse widths (0.1–10 ms), electroporation occurs. Electroporation is the formation of pores in the cell membrane as a result of an accumulation of charge at the surface of the cell membrane. This phenomenon then allows the delivery of genes or drugs to the interior of the cell. The voltage drop across the membrane typically needs to be between 0.1 and 1 V for electroporation to be important [24, 25].

If the electric field in the interior of the cell within the cytoplasm is on the order of tens of kV cm^{-1} and of short enough duration (10–100 ns), the charging time required for electroporation is not reached [26]. However, the intracellular substructure can be influenced by these electric fields through intracellular electromanipulation [25–28]. Experiments have shown that nano-pores may form from the short intense fields that are large enough to allow transfer of molecules and ions through the membrane of the cell [29, 30]. The membrane remains intact after the pulse. Vernier *et al* indicated that

these short voltage pulses move intracellular ions to localized regions (anode end) of the cell and promotes diffusion from the medium into the membrane [31]. More recent work has shown that short intense electric fields cause the mitochondria membrane to become permeable [32] and to activate mitogen-activated protein kinases (MAPKs) pathways [33] which influence intercellular communication. These nanosecond pulsed electric fields (nsPEF) have also been shown to induce apoptosis in *T* cells [31]. Other voltage regulated methods exist for external ions to enter the cells. Voltage-gated cation channels typically require a transmembrane voltage of up to 100 mV [34]. The movement of calcium and potassium cations by this method signals muscle contraction, propagates a nerve signal along an axon, or resets the cell back to equilibrium. There is also evidence that these impressed electric fields generate cell membrane temperature gradients, which in turn may contribute to electroporation through induced plasma membrane voltages [35]. Electric fields delivered by APPJs could potentially affect these processes. These ranges of electrical fields and the duration of the pulses investigated in bioelectronics are similar to those produced in plasma medicine for processes such as bacterial decontamination and wound healing.

The intent of the computational investigation reported on here is to determine if APPJs can create the conditions and deliver the electric fields required for electroporation, voltage-gated channels, or intracellular manipulation of cells when treating liquid covered tissue. The discharge characteristics and geometries analyzed were meant to approximate extreme, yet realistic, discharge conditions that could plausibly create these responses. The plasma conditions are a $\text{He/O}_2 = 99.8/0.2$ gas mixture excited by single discharge pulses flowing into humid air. The plasma plume is directed onto tissue covered by a thin layer of water. Idealized cells are at the surface of the tissue underlying the water and electric fields were examined in the cellular structure. We found that for conditions where the guided streamer or ionization wave from the APPJ does not touch the surface of the liquid, the electric fields induced in the tissue below the liquid layer are typically below a few kV cm^{-1} . These electric fields are not sufficient to produce significant electrical effects for the duration of the pulses investigated here. For conditions where the ionization wave does touch the surface of the liquid, electric fields of many tens of kV cm^{-1} may be produced in the cells for periods of many tens of ns. Although the duration of these electric fields may be too short to induce electroporation, they are commensurate with the electric fields required for intracellular electromanipulation.

The model used in this investigation is described in section 2, followed by a discussion of electric field penetration into the sub-liquid cells in section 3. Our concluding remarks are in section 4.

2. Description of the model

This modeling investigation of the electrical treatment of cells under thin water layers by an APPJ was conducted using *non-PDPSIM*, a plasma hydrodynamics model discussed extensively in [36]. The incorporation of a reactive water layer into the computational infrastructure is discussed in [37]. A 2D

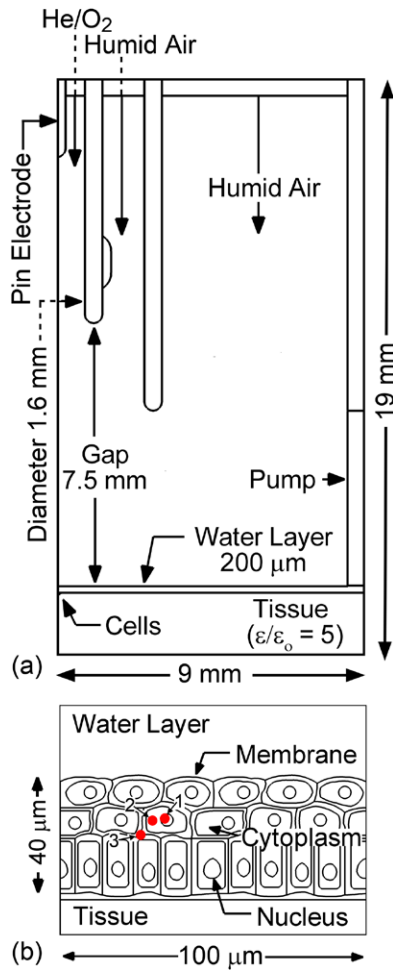


Figure 1. Schematic of the 2D Cartesian symmetric model geometry for a plasma jet incident onto a thin water layer overlying tissue. (a) The full computational domain is 19 mm tall by 9 mm wide. There is an optional electrode (not used here) on the outside of the inner tube. (b) Enlargement of the cells located on axis beneath the water layer at the surface of the tissue. The locations in the cells to be discussed are indicated by the numbered red dots: 1 = nucleus, 2 = cytoplasm, 3 = membrane.

Cartesian coordinate system was used to enable incorporating a tissue-like material having cellular structure beneath the water layer. The computational domain that is actually computed in the model is shown in figure 1(a) and is 9 mm wide \times 19 mm tall. The geometry is symmetric across the left border and so the domain represented by the model is 18 mm \times 19 mm. The figures show only the right-side of the symmetric results in order to show details as large as possible. Helium with 0.2% oxygen flowed through the inner tube having a diameter of 1.6 mm at 4 slm. The He/O₂ flow was shrouded by humid air (N₂/O₂/H₂O = 79.5/20/0.5) flowing at 1 slm. The flow in the tube for these conditions is laminar as the Reynolds number is less than 700, whereas the transition to turbulent occurs at a Reynolds number of about 2300. The jet into atmosphere also has a flow length significantly less than what is typically required to transition to turbulent [36, 38]. These gases flowed into humid air having the same composition as the shroud and exited at the side port labeled pump. The boundary condition at the face of the pump port is a constant pressure of 1 atm.

Table 1. Electrical Properties of the cell components.

	Permittivity (ϵ/ϵ_0)	Conductivity ($\Omega^{-1} \text{ cm}^{-1}$)	Dielectric relaxation time (s)
Membrane	5.8	8.7×10^{-8}	5.9×10^{-6}
Cytoplasm	30	4.8×10^{-3}	5.5×10^{-10}
Nucleus	20	3.0×10^{-5}	5.9×10^{-8}
Tissue	5	1.0×10^{-6}	4.4×10^{-7}

The top of the water layer was 7.5 mm from the end of the tube and in the base case the water layer was 200 μm thick. Evaporating water vapor above the liquid layer is included in the model. The thickness of the water layer represents the typical thickness of a biofilm [39].

The cells, shown in figure 1(b), were placed on the axis at the top of the tissue layer and cannot be distinguished at the larger scale of figure 1(a). The idealized cells are composed of a nucleus, cytoplasm, and membrane. Each component was modeled as a lossy dielectric with values for permittivity and conductivity shown in table 1. Expanding on a previous study on the effect of dielectric barrier discharges on skin and the underlying cells [40], the values of the permittivity and conductivity are based on those from an electroporation model [41] and dielectric spectroscopy [42, 43]. The dielectric relaxation time shown in table 1 is the dielectric constant divided by the conductivity (ϵ/σ). The dielectric relaxation time, τ_d , of the cytoplasm is less than 10 ns, which enables the possibility of intracellular electromanipulation and a cellular response to ultrashort pulsed electric fields.

The computational mesh has 26 600 nodes of which 17 000 are plasma nodes. The unstructured, triangular mesh has spacing of 36 μm at the tip of the electrode, 20 μm in the water layer, and smaller than 1 μm in the cells. The cellular structure consists of three layers of cells for a total thickness of 40 μm and width of 100 μm . This small collection of cells was selected to reduce the computational burden as this block of cells consists of over 6000 mesh points. The three layers are intended to show the effect of the propagation of the electric field through the cell layers.

Three voltage amplitudes (−10 kV, −15 kV, and −20 kV) and their interaction with cells lying beneath the 200 μm water layer were analyzed using voltage as a means to control whether the plasma touches the liquid. The water layer thickness was varied from to 50 μm to 1 mm using the −15 kV case as a baseline. The voltage pulse shape has a 5 ns rise to the applied voltage until 50 ns at which time the voltage decreases to zero over the next 10 ns. This duration of the voltage pulse is on the order of that required for intracellular electromanipulation [24, 32, 33]. Electroporation effects caused from accumulation of charge on cells are discussed using the predicted voltages and charging effects on the cell membrane.

3. Electric fields in cells produced by APPJs

The gas flow is first simulated to establish the steady state, laminar flow field prior to pulsing the plasma. The concentration

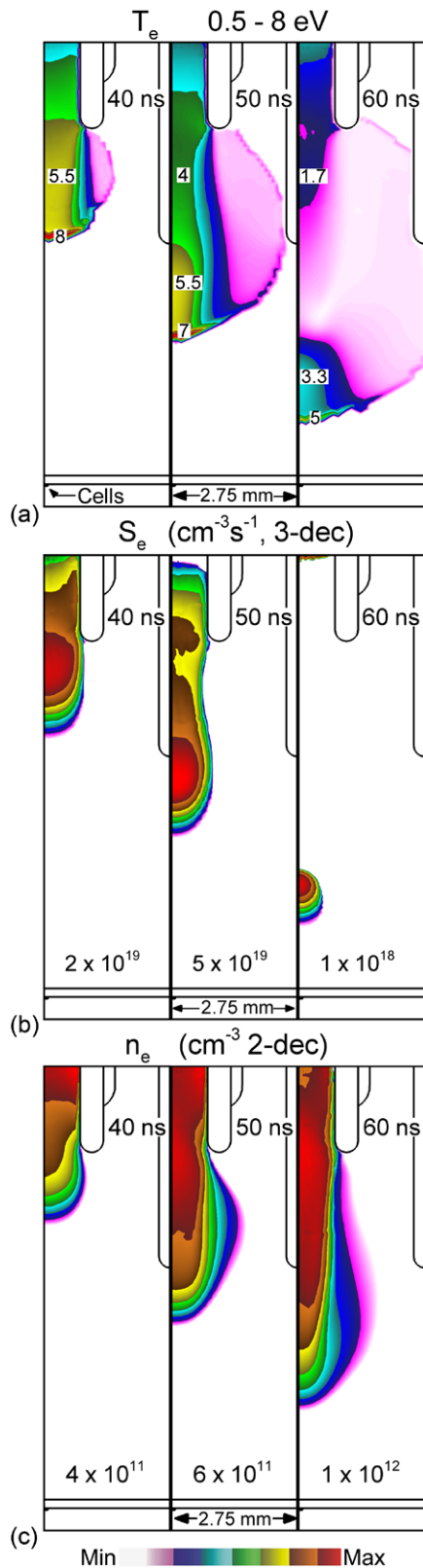


Figure 3. Plasma dynamics for the not-touching, -10 kV , plasma jet shown at the maximum of the applied potential at 40 and 50 ns and at zero applied voltage at 60 ns. (a) Electron temperature T_e on a linear scale between $0.5\text{--}8\text{ eV}$. (b) Electron impact ionization source S_e using a log-scale over three decades. (c) Electron density using a 2-decade log-scale. The maximum value in each frame is noted.

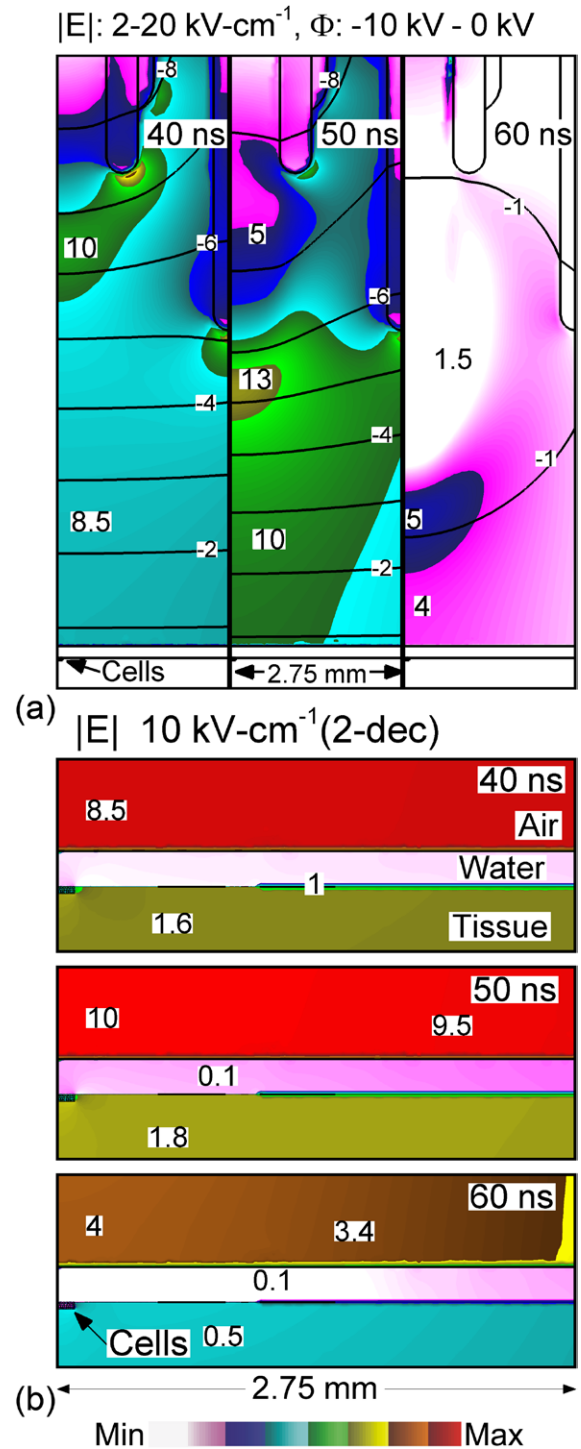


Figure 4. Magnitude of electric field for the not-touching, -10 kV , plasma jet at 40, 50 and 60 ns. (a) Electric field using a linear scale from $2\text{--}20\text{ kV cm}^{-1}$ with potential contours representing one kV changes. (b) Electric field at the air–water layer–tissue interface for a maximum of 10 kV cm^{-1} over two decades.

3.2. -15 kV : base case touching APPJ

By increasing the applied voltage to -15 kV , an increase in the speed of the guided IW enables the discharge to touch the water layer during the 60 ns voltage pulse. T_e , S_e and

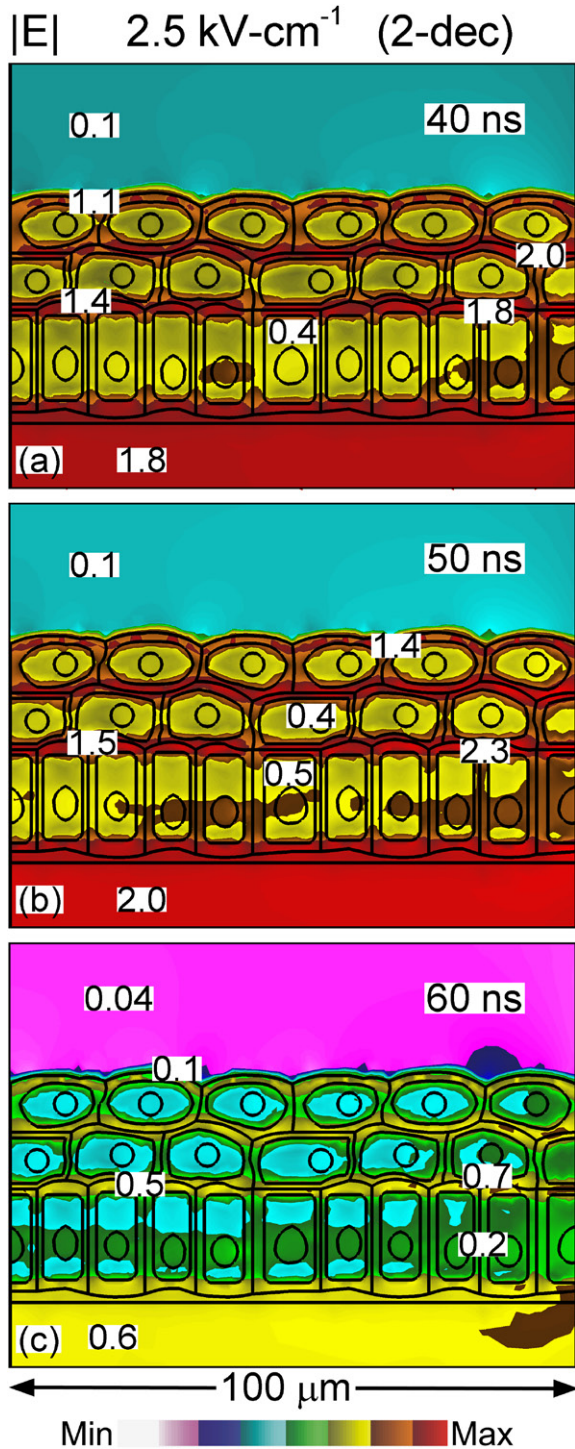


Figure 5. Magnitude of electric field for the not-touching, -10 kV , plasma jet at 40, 50 and 60 ns at the water layer—cell membrane interface, within the cell structure, and in the tissue below the cell. Electric fields have a maximum of 2.5 kV cm^{-1} and are shown on a log-scale over two decades.

n_e for this base case are shown in figure 6 as the IW propagates through the helium channel -3 ns before touching the water layer (29.5 ns), at the moment of touching (32.5 ns), and 3 ns after the IW touches the water layer (35.5 ns). T_e is as high as 9 eV at the front of the ionization wave which travels at a speed of $8 \times 10^7\text{ cm s}^{-1}$. The electrons form a

conducting channel upon touching the water and increase in density to 10^{13} cm^{-3} . Since on the time scale of the discharge pulse, the water is essentially a dielectric (τ_d is much longer than the discharge pulse), electrons and ions accumulate on the surface of the water and produce a surface electric field as they solvate or charge exchange into the water layer. The maximum electron density occurs on axis at the surface of the water layer at 35.5 ns. Due to the charging of the surface of the water, the discharge operates similarly to a dielectric barrier discharge (DBD). S_e splits into two sections, with one component spreading across the surface of the water layer as a surface ionization wave (SIW), and the other component acting as a restrike travelling back up the helium channel towards the electrode.

The electric fields and electric potentials in the gas phase, through the water layer and in the cells for the base case are shown in figures 7 and 8 for times of 3 ns before the APPJ touches, at the moment of touching and 3 ns after touching. As the IW travels through the He plume, the space charge enhanced electric field at the head of the IW increases in intensity. Halfway through the gap (29.5 ns), the electric field in the head of the IW is 24 kV cm^{-1} . At this time, the electric potential contours are not strongly compressed in front of the ionization wave. As the IW strikes the surface at 32.5 ns, the compression of the electric potential against the high capacitance and high permittivity water layer, and charging of the surface increases the electric field at the head of the streamer to 44 kV cm^{-1} . The low magnitude of the electric field behind the IW at 35.5 ns is due to the high conductivity of the plasma channel and enables more of the applied potential to be dissipated in the water and liquid.

When the IW strikes the surface of the water layer, charging of the surface is rapid and the resulting electric field penetrates through the water layer and into the tissue to a maximum magnitude of 14 kV cm^{-1} at 35.5 ns. This charging is, however, a local phenomenon. The electric field at the air/water interface above the cells (to a width of 2.75 mm) is shown in figure 7(b) at times of 3 ns before touching, at touching, and 3 ns after touching. Prior to the IW touching the water layer (29.5 ns), the electric field above the water is 17 kV cm^{-1} , corresponding to a fully realized -15 kV potential over a distance from the electrode to the water of nearly 1 cm. There is little effect of the discharge on or in the water layer at this point. At touching, 32.5 ns, the electric field at the surface of the water layer increases to 44 kV cm^{-1} and there is a rise in the magnitude of the electric field in both the water and the tissue beneath to 1 kV cm^{-1} and 5 kV cm^{-1} , respectively. The large electric field at the surface results from charging of the surface. At this point, -13 kV is dissipated in the plasma column on axis. At 3 ns after touching, the potential remaining in the plasma column is 11.5 kV on axis. The intense electric field at the surface of the water layer is largely dissipated by current flowing from the now continuous plasma column from the electrode to the surface. At this point, the magnitude of the electric field is 14 kV cm^{-1} in the tissue and 5 kV cm^{-1} in the water layer. As the SIW begins to propagate outward on top of the water layer, the region of most intense electric field in the water layer and in the tissue also translates outwardly.

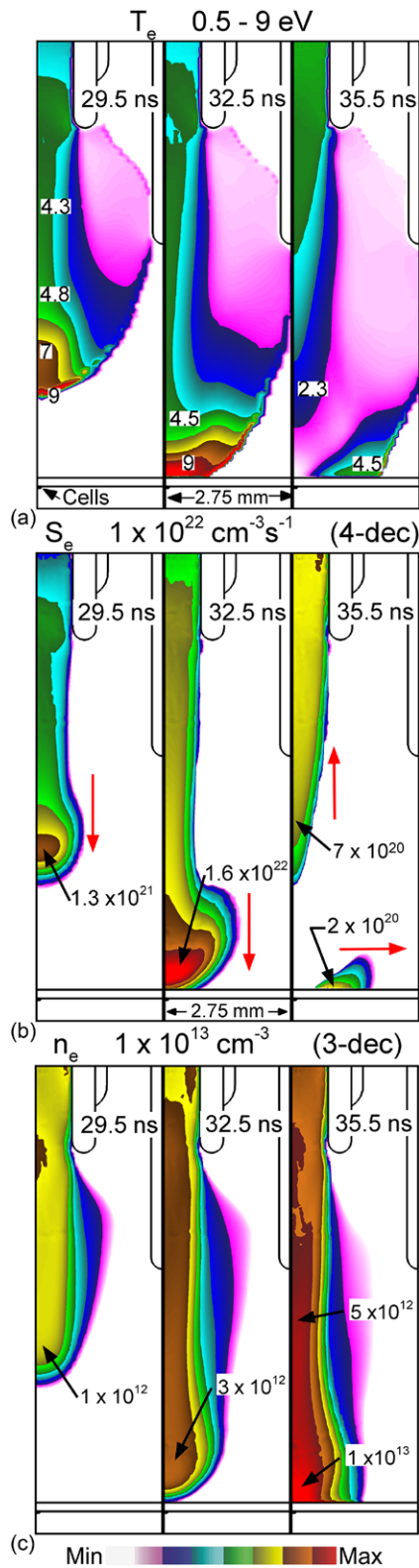


Figure 6. Plasma dynamics for the touching, -15 kV , plasma jet shown at 3 ns before touching (29.5 ns), at touching (32.5 ns), and 3 ns after touching (35.5 ns). (a) Electron temperature T_e , using a linear scale from 0.5–9 eV. (b) The electron impact ionization source S_e , using a log-scale over four decades from a maximum of $10^{22} \text{ cm}^{-3} \text{ s}^{-1}$. The directions of propagation of the IW or SIW are shown by arrows. (c) Electron density n_e , using a log-scale over three decades from a maximum of 10^{13} cm^{-3} . The formation of the conduction channel is apparent at 35.5 ns.

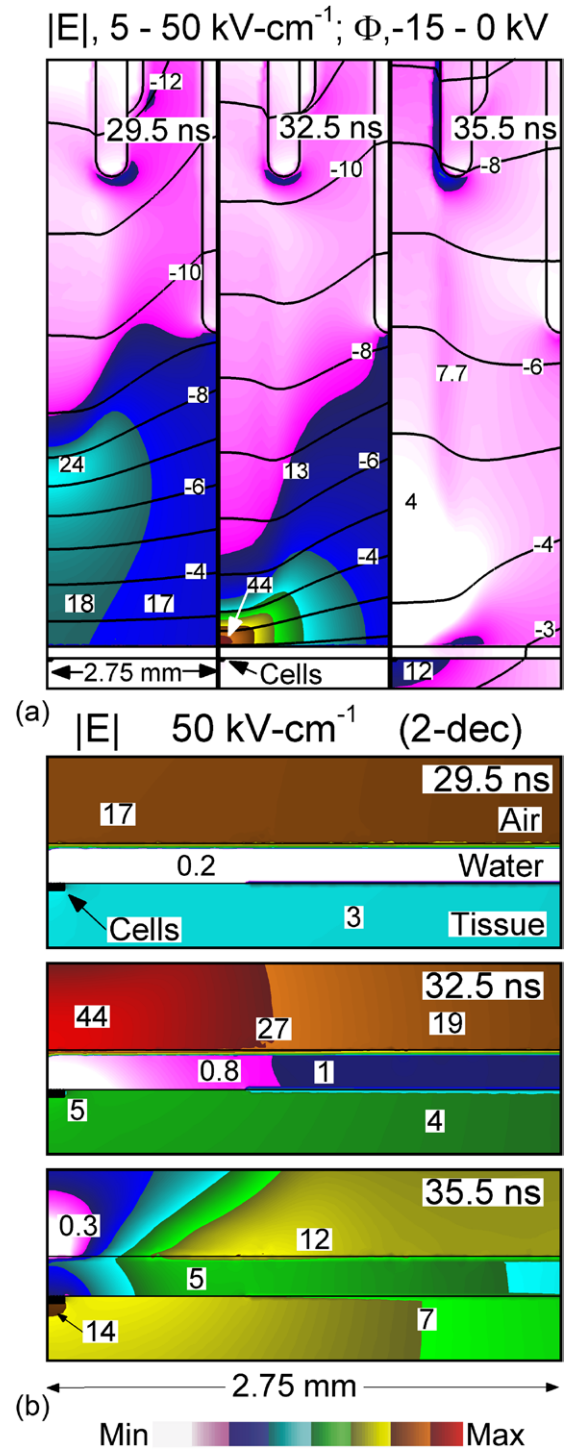


Figure 7. Magnitude of electric field for the touching, -15 kV , plasma jet at 3 ns before touching (29.5 ns), at touching (32.5 ns), and 3 ns after touching (35.5 ns). (a) Electric field using a linear scale from 5–50 kV cm^{-1} with potential contours representing 1 kV changes. (b) Electric field at the air–water layer—tissue interface from at 3 ns before, at touching to 3 ns after touching using a log-scale from a maximum of 50 kV cm^{-1} over two decades.

The cells, too small to be clearly seen in figure 7, are shown in figure 8. As the ionization wave approaches (29.5 ns), the electric fields in the cells vary from 0.8 kV cm^{-1} in the cytoplasm and 1.1 kV cm^{-1} in the nucleus, to 2.2 kV cm^{-1} in the cell membranes. Note that the electric field is larger on the

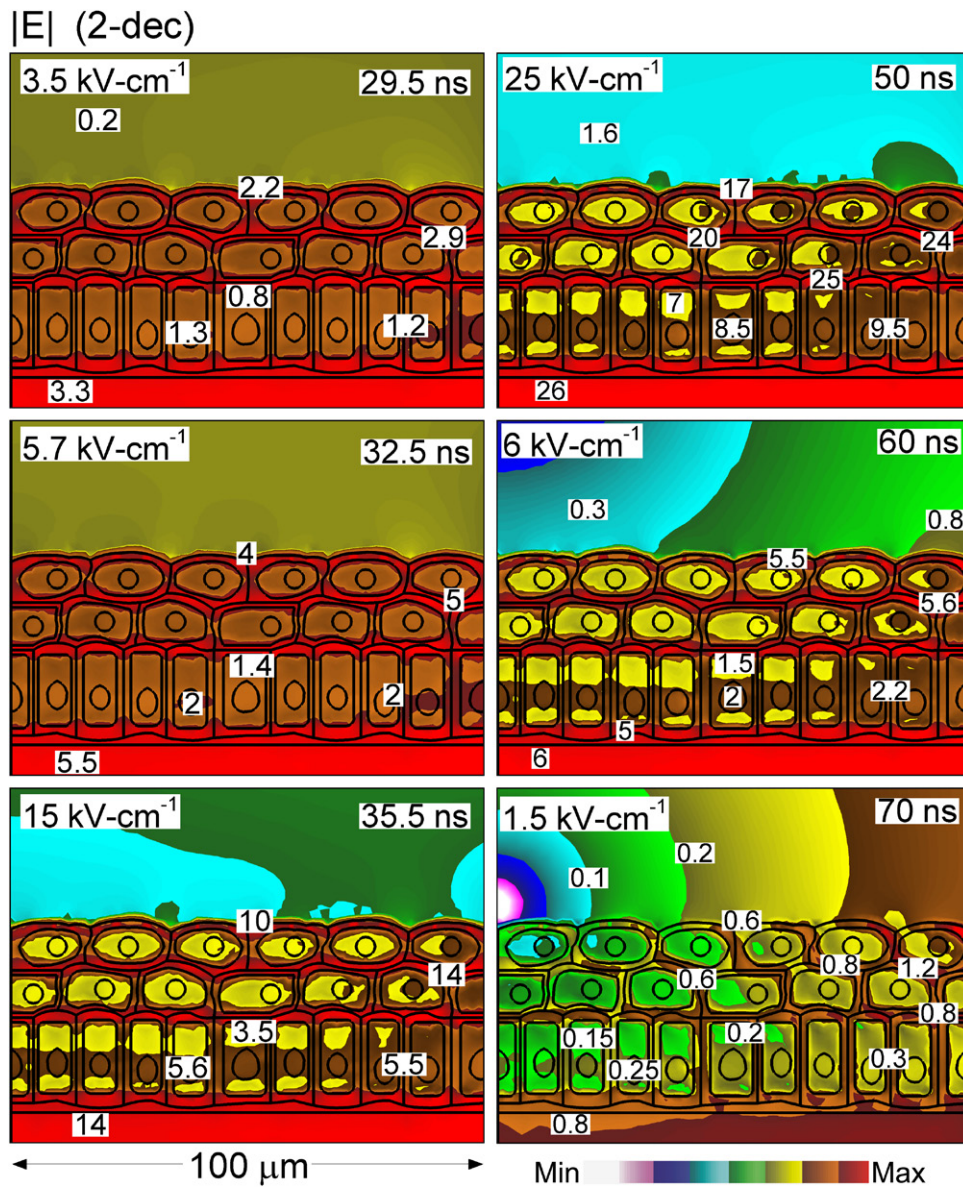


Figure 8. Electric field magnitude at the water layer–cell membrane interface, within the cell structure, and in the tissue below the cells for the -15 kV plasma jet. Values are shown (left column) 3 ns before, at touching and 3 ns after touching; and (right column) at the maximum extent of the pulse at 50 ns, the end of the voltage pulse 60 ns, and 10 ns into the afterglow at 70 ns. The maximum electric field is shown in each frame for a two-decade range in values.

horizontal membranes (2.2 kV cm^{-1}) than on the vertical cell membranes (1.2 kV cm^{-1}). Since the electric field on axis is largely vertically oriented, polarization due to charge motion in the cytoplasm is dominantly in the vertical direction, which results in charging of horizontally oriented surfaces more than vertically oriented surfaces. Three nanoseconds after touching, the electric field in the membrane is between 5.5 kV cm^{-1} (vertical membranes) and 12 kV cm^{-1} (horizontal membranes). The cytoplasm has a higher conductivity and higher dielectric constant than the membrane and so experiences a lower electric field of 3.5 kV cm^{-1} . At this time, the nucleus with a dielectric constant and conductivity between that of the membrane and cytoplasm experiences an electric field as high as 5.0 kV cm^{-1} in the third row of cells. Beneath the cells, the electric field in the tissue is 14 kV cm^{-1} . At this point, within the first 3 ns of the IW striking the surface,

the electric fields are of sufficient magnitude but too short a duration to produce electroporation. The electric fields are too low to promote intracellular electromanipulation.

The electric fields are shown in figure 9 as the applied voltage is removed—at 50 ns (the extent of the maximum voltage pulse), 60 ns (when the applied voltage terminates) and 70 ns (10 ns into the afterglow). At 50 ns, the electron density in the conduction channel is $1.3 \times 10^{13} \text{ cm}^{-3}$ and is $2 \times 10^{13} \text{ cm}^{-3}$ in the SIW as it spreads across the water surface. The higher, off-axis electron density results from the SIW intersecting the region of higher water vapor density, as shown in figure 2. The conducting channel from the pin electrode to the surface decreases the electric field in the column to 1 kV cm^{-1} . The confining ambipolar space charge field at the radial boundary of the plasma column produces electric fields of $2\text{--}3 \text{ kV cm}^{-1}$. At 60 ns as the voltage is removed,

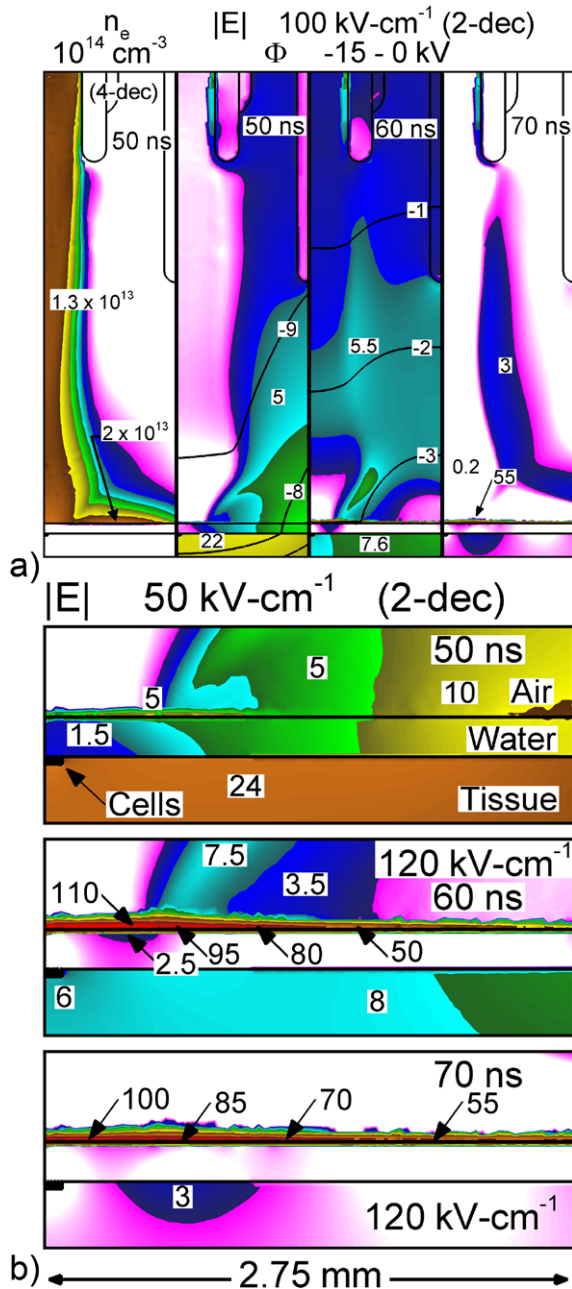


Figure 9. Plasma dynamics for the end of the pulse for the -15 kV plasma jet. (a) Electron density at 50 ns on a log-scale over four decades; and the magnitude of the electric field and potential contours at 50, 60 and 70 ns. The contours represent 1 kV and the electric field is shown using a log-scale from 100 kV cm^{-1} over two decades. (b) The electric field at the air–water layer–tissue interface at the maximum extent of the voltage pulse (50 ns), end of the voltage pulse (60 ns) and 10 ns into the afterglow (70 ns). Note the large electric field forming in a sheath at the surface of the liquid. The roughness of this region of high electric field is an artifact of the plotting.

the remaining space charge produces an electric field at the boundary of the conduction channel with a magnitude of 5.5 kV cm^{-1} . As the voltage further decreases and electrons attach to form low energy negative ions, the ambipolar electric field decreases. By 70 ns, the ambipolar field has fallen to 3 kV cm^{-1} at the periphery of the plasma column where the

remaining space charge is largest. The spread of the ionization wave across the water layer and the electric field due to surface charge ($60\text{--}100 \text{ kV cm}^{-1}$ along the surface) are shown at the air/water interface in figure 9(b). The extent of the local electric field due to surface charging corresponds to the spread of SIW across the water surface. At 70 ns, there is no remaining applied voltage, however the charge remaining on the surface of the water sustains a local, spatially varying electric field that penetrates into the tissue.

The electric field in the cell structure beneath the water layer as the voltage decreases is shown in figure 8. At the end of the maximum of the voltage pulse, the cell membrane experiences an electric field ranging from 10 kV cm^{-1} (vertical membranes) to 25 kV cm^{-1} (horizontal membranes), whereas the electric fields for the cytoplasm and nucleus are 7 kV cm^{-1} and 8.5 kV cm^{-1} . With the termination of the voltage at 60 ns, the electric fields in the membranes are 5.5 kV cm^{-1} (horizontal) and 2.2 kV cm^{-1} (vertical), and those in the cytoplasm and nucleus are 1.5 kV cm^{-1} and 2 kV cm^{-1} , respectively. At 70 ns, or 10 ns after the pulse, there are two sources of electric fields for the cells. The first is the internal charging of cellular structures that resulted from charge motion in the cytoplasm and polarization during the discharge pulse. With $\tau_a \approx 1\text{--}100$ ns for the cytoplasm and surrounding membranes, the charged membranes begin to dissipate and the electric fields in the cells quickly fall below 1 kV cm^{-1} . The second is the large electric field at the surface of the water due to the persistent surface charging. The nonuniformity in the electric fields in the cells in large part results from the maximum in surface charge and electric field that occurs to the right of the cells.

The electric field and voltage across a 10 nm membrane dissipates quickly in the 10 ns afterglow and does not provide sufficient intensity for a long enough period of time to promote electroporation. The predicted electric fields in the cytoplasm are still below the intracellular electromanipulation threshold.

3.3. -20 kV: touching APPJ

Increasing the applied voltage to -20 kV directly results in a faster and more intense ionization wave touching the water layer at 20 ns, 13 ns earlier than the -15 kV case with a propagation speed of $1.3 \times 10^8 \text{ cm s}^{-1}$. T_e at the time the IW strikes the surface (20 ns), and S_e and n_e at 23 ns are shown in figure 10. T_e reaches 11 eV while n_e increases to $3 \times 10^{13} \text{ cm}^{-3}$ at the surface upon formation of the conduction channel. The IW that propagates along the surface of the water layer has an ionization source ($1 \times 10^{21} \text{ cm}^{-3} \text{ s}^{-1}$) that is an order of magnitude higher than the -15 kV case.

The electric fields produced with a -20 kV pulse generally follow the same trends as for the base case. As in the base case, charge on the surface of the water layer produces a local electric field in excess of 100 kV cm^{-1} at the point where the IW touches the surface at the end of the discharge pulse. At the extent of the spread of the SIW, the electric field at the surface is 30 kV cm^{-1} . At this time, the electric fields in the horizontal cell membranes are $25\text{--}35 \text{ kV cm}^{-1}$ and $13\text{--}15 \text{ kV cm}^{-1}$

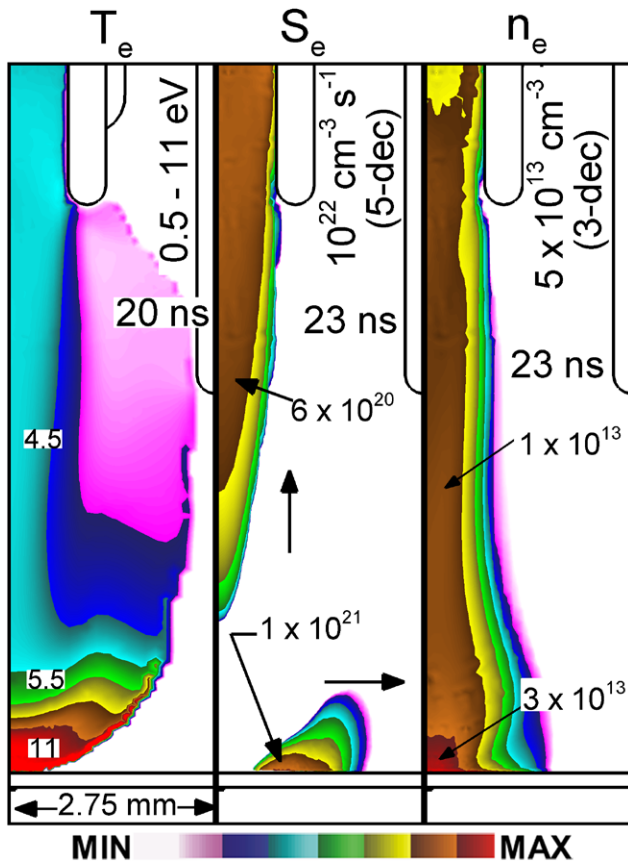


Figure 10. The critical discharge dynamics of the touching, -20 kV , plasma jet. (left to right) Electron temperature T_e , using a linear scale from $0.5\text{--}11\text{ eV}$ when the guided ionization wave touches the water layer at 20 ns ; the electron impact ionization source S_e , using a log-scale over five decades 3 ns after touching; and electron density n_e , using a log-scale over three decades at 3 ns after touching. The arrows indicate the direction of the restrike and surface ionization wave.

in the vertical cell membranes, as shown in figure 11. The electric field reaches 9 kV cm^{-1} in the cytoplasm, and 13 kV cm^{-1} in the nucleus at the end of the high voltage pulse (50 ns). These values for electric field in the cytoplasm are nearly at the threshold for intracellular electromanipulation, 10 kV cm^{-1} . A number of system variables, could raise the interior electric field above the low end of the intracellular electromanipulation threshold, such as a slight increase in voltage or pulse duration, or the cumulative effects of pulse repetition on the aqueous species in the water layer or charge accumulation on the cells. The voltage across a 10 nm membrane, 0.035 V , is still, however, below the critical voltage for electroporation.

As the voltage decreases to zero and then into the afterglow, and the charge on the cell membranes dissipates, the electric fields in the cells decrease to a few hundred V cm^{-1} by 70 ns . The surface charging is, on a relative basis, larger at larger radius than for the base case, and so produces an asymmetry in the electric fields induced in the cells. This results in a large horizontal component of the surface-charge-generated electric field at the location of the cells. This electric field in turn polarizes the cells such that the vertical membranes

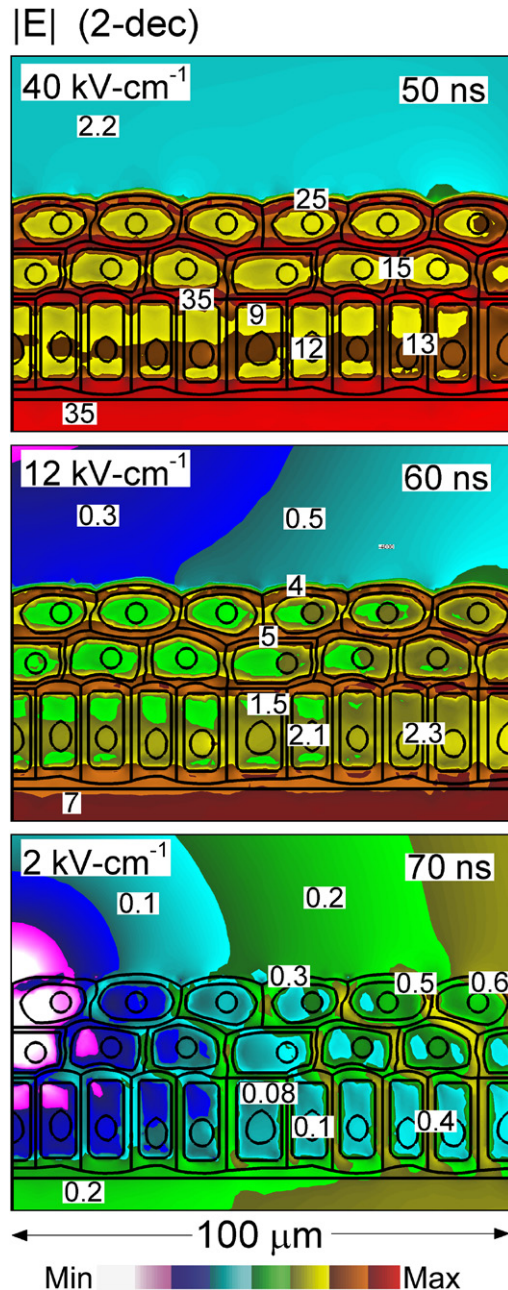


Figure 11. The magnitude of the electric field at the air–water layer–tissue interface for the -20 kV plasma jet at the end of the high voltage portion of the pulse (50 ns), at the end of the applied voltage (60 ns) and 10 ns into the afterglow (70 ns). The maximum electric field is shown in each frame for a two-decade range.

have comparable electric fields compared to the horizontal components.

3.4. Second -15 kV pulse

The effect of a more conductive water layer was investigated by allowing the aqueous reactions resulting from the first -15 kV pulse onto the $200\text{ }\mu\text{m}$ water layer to continue for 50 ms and then applying a second -15 kV pulse. This technique is similar, though on a shorter timescale, to the nanosecond pulsed electric field (nsPEF) cases investigated by Schoenbach *et al* [25]

in which 20 individual 80 ns pulses occurred at a frequency of 1 Hz. The density of charged species that remained in the water layer ranged from nearly $1 \times 10^{14} \text{ cm}^{-3}$ at the surface of the water layer to nearly $1 \times 10^{10} \text{ cm}^{-3}$ at the tissue. For a charged particle density of 10^{13} cm^{-3} , the conductivity of the resulting liquid is $3 \times 10^{-5} \Omega^{-1} \text{ cm}^{-1}$. The accumulation of charge on the surface (density of 10^{14} cm^{-3}) produces a higher conductivity ($3 \times 10^{-4} \Omega^{-1} \text{ cm}^{-1}$). This is an increase of nearly two orders of magnitude in conductivity from the water subjected to the first pulse. Over the interpulse period of 50 ms, the gaseous reactive species have moved out of the domain of interest with the flowing helium and the second pulse enters into a nearly pristine gaseous environment.

The resulting discharge dynamics of the second pulse visually appear nearly the same as the first pulse, though there are quantitative differences. The IW strikes the more conductive water layer nearly 3 ns later than the first pulse. The higher conductivity of the water layer distributes potential along the surface more uniformly, which then reduces the vertical electric field and produces a larger horizontal component away from the surface. The vertical speed of the IW and ionization source in the plasma column therefore decrease. Along the more conductive surface, the horizontal component of the electric field that sustains the SIW decreases. This decrease in horizontal component of the electric field then decreases the electron impact ionization source term, S_e , along the surface from $2 \times 10^{20} \text{ cm}^{-3} \text{ s}^{-1}$ at 3 ns after the first pulse to $9 \times 10^{19} \text{ cm}^{-3} \text{ s}^{-1}$ at 3 ns after the second. These are not large differences but do reflect the changes in the electrical environment into which the IW propagates.

At the end of the pulse and into the afterglow, some differences appear. The electron density at the end of the maximum applied voltage (50 ns) is lower in both the conductive channel ($4 \times 10^{12} \text{ cm}^{-3}$ versus $1.3 \times 10^{13} \text{ cm}^{-3}$) and on the surface of the water layer ($8 \times 10^{12} \text{ cm}^{-3}$ versus $2 \times 10^{13} \text{ cm}^{-3}$) compared to the first pulse. The spread of the electrons on the water layer is also reduced, resulting in the extent of the charged surface decreasing from 2.5 mm to 1.5 mm at 60 ns.

Within the cells the electric fields during the second pulse at 50 ns are visually similar to those for the first pulse but with overall smaller magnitudes. For example, for the same locations, the electric fields in the horizontal membranes decrease from 25 kV cm^{-1} for the first pulse to 21 kV cm^{-1} for the second pulse. In the cytoplasm the decrease is from 7 kV cm^{-1} to 5.3 kV cm^{-1} , and in the nucleus from 8.5 kV cm^{-1} to 7.6 kV cm^{-1} . There is some shielding of the cells that occurs by the now more conductive overlying liquid layer. At the end of the second pulse, the conclusions concerning electrical effects induced in the cells are the same as after the first pulse. There is little likelihood for electroporation and a small possibility of intracellular electromanipulation.

3.5. Time evolution of electric fields

The time evolution of the electric field at the surface of the water layer, within the cell membrane, cell cytoplasm and cell nucleus are shown in figure 12 for the four cases discussed. Above the surface of the water layer, 10 μm from the centerline,

the initial rise in electric field results from the initial increase of the applied potential. The electric field then remains relatively constant until the IW approaches within a few mm of the surface. As the conductive plasma extends towards the surface, the applied electric potential is compressed into the low conductivity gas and liquid in front of the more conductive IW, thereby increasing the electric field. For -15 kV and -20 kV , the electric field sharply increases as the space charge in front of the IW is transferred to the surface of the water upon touching.

When the IW then touches the surface, a conductive channel then exists between the electrode and the surface, resulting in the applied potential being fairly uniformly distributed across the plasma column. This uniform distribution of potential then reduces the electric field above the water while continuing to charge the surface of the water. As the voltage begins to decrease at 50 ns to zero at 60 ns, the plasma which shields the electric field produced by surface charging begins to decay while charge continues to be collected on the surface. This produces a large electric field in front of the water layer resulting from a sheath like structure. Electrons are rapidly solvated into the liquid compared to the positive ions. The charge of the solvated electrons remains at the surface producing negative space charge while the adjacent plasma is depleted of electrons producing positive space charge. Note that this high electric field is only adjacent to the plasma-liquid interface. This process is analogous to a dielectric barrier discharge where upon termination of the applied voltage pulse potential is transferred to the opposite dielectric surface that had been charged during the discharge pulse. In the afterglow from 60 ns to 70 ns, the magnitude of the electric field at the surface decreases as diffusion of ions from the gas phase into the liquid and diffusion of solvated electrons into the water reduces the surface charging. The trends for the 2nd pulse for -15 kV are similar to the first pulse.

The electric fields for the -10 kV pulse show only the consequences of compression of the electric potential in front of the IW as the IW only partially crosses the gap. In the absence of touching the surface, there is no conduction current to the surface from the IW and so negligible surface charging to produce the large electric fields observed in the -15 kV and -20 kV cases.

Electric fields within the cellular structure are also shown in figure 12 at the points indicated in figure 1(b). The electric fields generally scale with the applied voltage for -15 kV and -20 kV . In the absence of surface charging, the intracellular electric fields for -10 kV are generally $< 1 \text{ kV cm}^{-1}$. For the -20 kV case, the electric fields in the membranes initially rise to 24 kV cm^{-1} . In the more conductive cytoplasm and nucleus, the initial increases are to 7.7 kV cm^{-1} and 8.3 kV cm^{-1} . These abrupt increases in electric field coincide with the arrival of the IW onto the surface of the water and charging of the surface. The second rise in the magnitude of the electric field beginning at 30 ns results from the continuing charging of the surface of the water. At the end of the maximum applied voltage at 50 ns, the electric field in each cellular region decreases towards zero, which is in the opposite direction from the electric field directly above the liquid layer due to lack of the sheath-like structure.

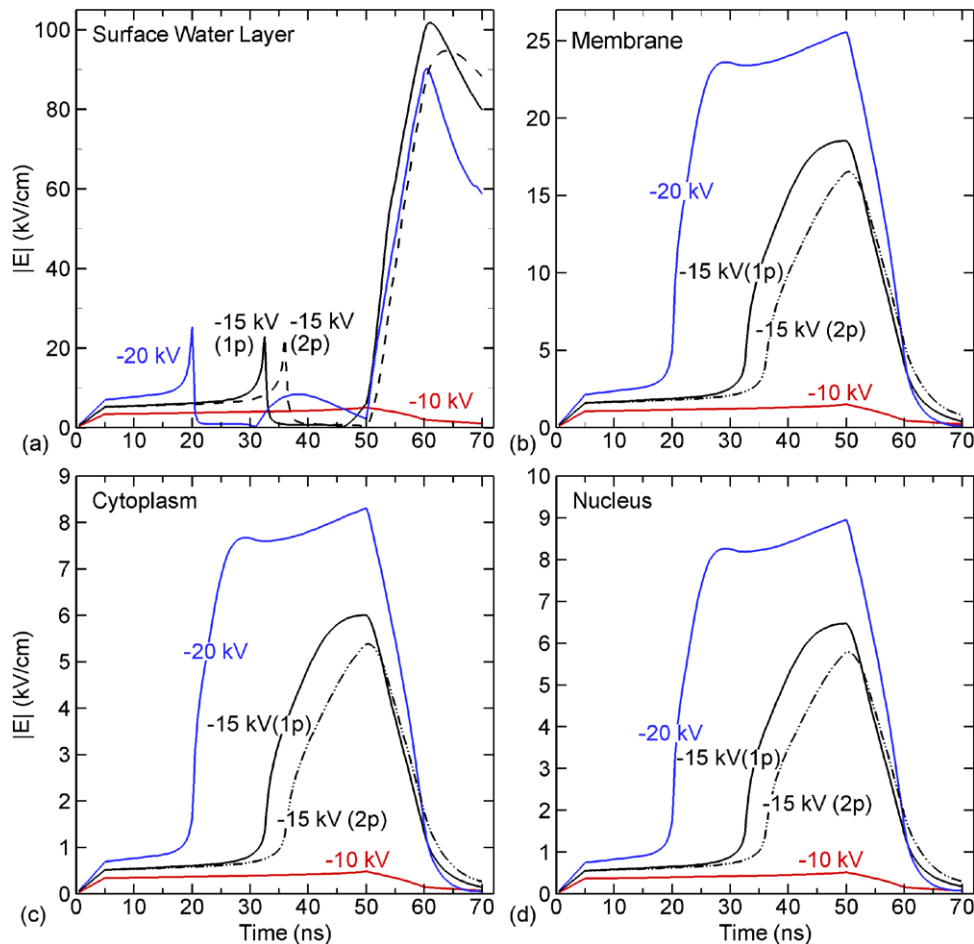


Figure 12. The magnitude of the electric field as a function of time at four locations for the -10 kV, -15 kV (1st pulse (1p) and 2nd pulse (2p)) and -20 kV plasma jets for a $200\ \mu\text{m}$ water layer. (a) In the sheath at the surface of the water layer, $10\ \mu\text{m}$ from the centerline, (b) in the cell membrane, (c) in the cytoplasm and (d) in the nucleus. The locations of the electric fields for the membrane, cytoplasm and nucleus are indicated in figure 1(b).

During the fall of the applied voltage, the electric field in the membrane, cytoplasm and nucleus at the end of the second pulse increase to values above those during the first pulse. The accumulation of charge and the presence of charged species in the water layer do have a measurable effect on the electric fields seen by the underlying cells.

3.6. Water layer thickness (50 and 1000 μm)

Using the same voltage (-15 kV) waveform, electric fields were investigated as the thickness of the water layer was decreased from $200\ \mu\text{m}$ to $50\ \mu\text{m}$ and increased to $1000\ \mu\text{m}$ (1 mm). In order to reduce the magnitude of the calculation, the reactive portion of the water layer was reduced to a half-width of $2.75\ \text{mm}$ (corresponding to the radius of the tube for the shielding gas). The remainder of the water layer was treated as a dielectric having $\epsilon/\epsilon_0 = 80$. In order to compare the results to the base case, a $200\ \mu\text{m}$ case with the same geometric modifications was modeled as well. No major changes were seen between $200\ \mu\text{m}$ case with the truncated reactive water layer and the complete reactive water layer, as discussed in the earlier sections.

The discharge dynamics of the IW are affected by the thickness of the water layer due to the change in the series

capacitance represented by the water. A thicker water layer represents a smaller capacitance. The smaller capacitance charges more rapidly and produces a larger electric field in the sheath above the water, but also reduces the voltage drop across the gap more rapidly. This produces a slower, less intense surface ionization wave. A thinner water layer represents a larger capacitance which charges more slowly and produces a smaller electric field in the sheath. The voltage across the gap is larger for a longer period of time, which in turn produces a faster, more intense SIW.

The charging of the surface layer and the speed of the SIW produce somewhat compensating effects on the penetration of the electric field into the cells. Although there are systematic changes in the electric fields with thickness of the water layer, the maximum electric fields in the cells underlying the water are not significantly sensitive to the thickness of the water layer between $50\ \mu\text{m}$ and $1000\ \mu\text{m}$. For example the electric field in the sheath above the water, and electric fields in the membrane, cytoplasm and nucleus of the underlying cells are shown in figure 13. The maximum electric fields in the sheath increase from $50\ \text{kV cm}^{-1}$ to $170\ \text{kV cm}^{-1}$ as the thickness of the water layer increases from $50\ \mu\text{m}$ to $1000\ \mu\text{m}$. Although this scaling reflects the decreasing RC time constant

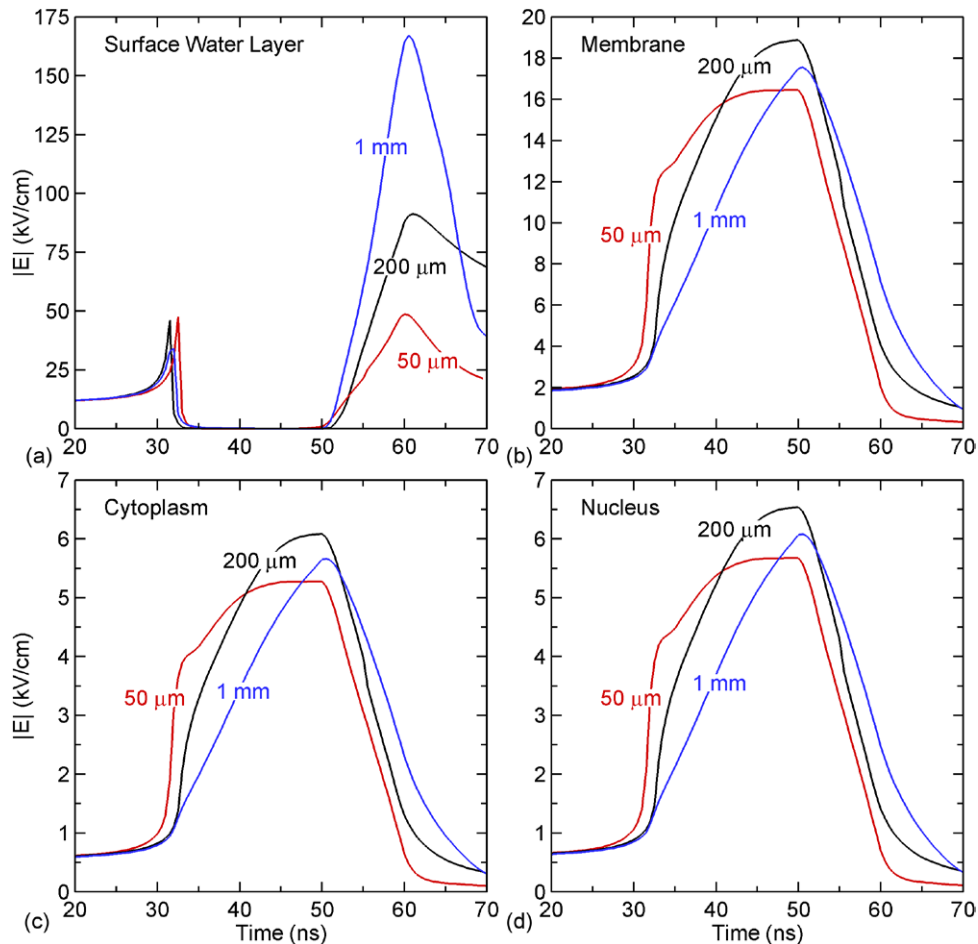


Figure 13. The magnitude of the electric field as a function of time at four locations for the -15 kV plasma jet for $50\ \mu\text{m}$, $200\ \mu\text{m}$ and $1000\ \mu\text{m}$ water layers. (a) In the sheath at the surface of the water layer, $10\ \mu\text{m}$ from the centerline, (b) in the cell membrane, (c) in the cytoplasm and (d) in the nucleus. The locations of the electric fields for the membrane, cytoplasm and nucleus are indicated in figure 1(b).

for charging of the water layer with increasing thickness, the scaling is sub-linear (a 20 times decrease in capacitance produces 3 time increase in electric field). This scaling results in part from a saturation effect in that when the surface fully charges the electric field does not continue to increase. There is also a dynamic associated with the spread of the SIW, discussed below.

The time dependence of the electric fields within the cell structure vary with water layer thickness, as shown in figure 13. The thin water layer, having a larger capacitance, enables the voltage and electric field to propagate to the cells earlier. The thicker water layers, having the smaller capacitance, charges more rapidly retaining potential above the cells and so delivers electric fields to the cells more slowly. The maximum values of the electric fields in the cells are not significantly different for different thickness, as those values of electric field are determined by the charging of the water layers to near the applied voltage (as in conventional DBDs), which eventually occurs for all thicknesses.

The details of the time dependence of the intracellular electric fields for different water layer thicknesses results, in part, from the spatial dependence of charging the water layer which depends on the speed of the SIW. The electric fields for the $50\ \mu\text{m}$ and $1000\ \mu\text{m}$ layers at 40 and 50 ns are shown in

figure 14. These are times when the intracellular electric fields are continuing to increase for the $1000\ \mu\text{m}$ layer and have leveled off for the $50\ \mu\text{m}$ layer. Note that the cells are below the water layer on axis and are too small to be clearly seen in the figures. The location of the SIW is indicated by the region of low electric field at the surface, followed by a large electric field where avalanche is occurring. The speed of the SIW is higher for the $50\ \mu\text{m}$ layer, and so the region of high electric field at the front of the SIW has moved away from the cells. The slower speed of the SIW for the $1000\ \mu\text{m}$ layer produces a longer dwell time in the vicinity of the cells.

4. Concluding remarks

The electric fields produced by an atmospheric pressure plasma jet modeled by a single pulse (or two pulses) onto thin water layers with underlying cells were investigated while varying the applied voltage and thickness of the water layer. We found that if the ionization wave of the plasma jet does not touch the surface of the water layer, the electric fields in the cells do not exceed a few kV cm^{-1} , and there is little likelihood of any significant electrical effects on the cells. When the ionization wave strikes and spreads on the water layer, electric fields exceeding tens of kV cm^{-1} were induced in

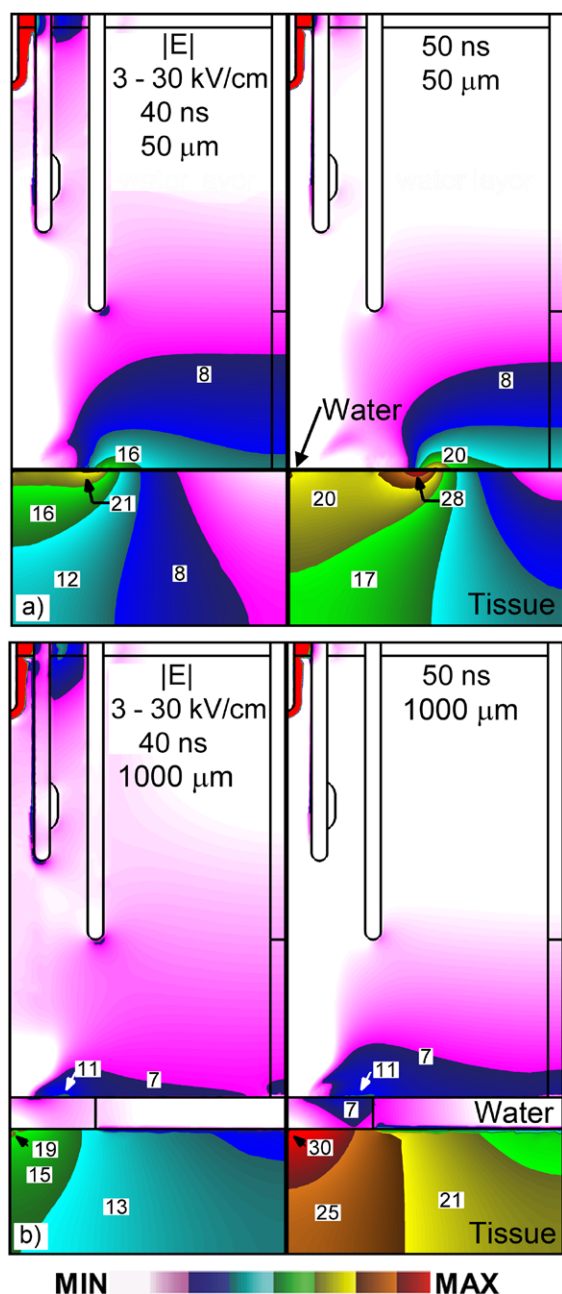


Figure 14. Propagation of the electric field in and through the tissue beneath the water layer for (a) 50 μm and (b) 1 mm thick water layers cases at 40 and 50 ns. The electric field is plotted on a linear scale for 3–30 kV cm^{-1} to highlight the electric field within the tissue.

cell membranes and up to 10 kV cm^{-1} in the cell nucleus and cytoplasm. For the 60 ns pulse duration investigated here, the values and durations of the electric field are not large enough to promote either electroporation or stimulating voltage-gated channels in the membranes. On the other hand, with the short duration and relatively high electric field produced in the cytoplasm, intracellular electromanipulation is possible. For certain conditions, we have concluded that the electric fields produced by the APPJ likely do not have significant effects on the cells. This conclusion does not imply that the APPJ has no effects at all. The reactive species, radiation and heating

resulting from the APPJ can clearly affect the cells in the absence of the electric fields.

There was an unexpected lack of sensitivity of the maximum electric fields in the cells when varying the thickness of the water layer from 50 μm to 1 mm. Although the time and spatial dynamics are sensitive to the thickness of the water layer, the maximum electric fields are only weakly dependent on thickness. This lack of sensitivity is, for the conditions investigated here, likely due to the charging of the surface of the water being similar for all thickness. With an increase in the number of pulses, increase in conductivity in the solution through pulsing, application to dry cells, and/or increase in voltage, intracellular electromanipulation is definitely plausible based on the predicted thresholds. Note that this study addressed electric fields delivered by plasma jets through an overlying liquid, with the plasma touching or not touching the liquid. The cells are not directly exposed to the plasma. The electric fields delivered to cells with the plasma touching the cells can be significantly larger and well above the electroporation limit [40].

Our computed results and conclusions are, to some extent, system specific. However, with respect to the penetration of electric fields into cells, the specific details of the in-liquid chemistry are not that critical unless the conductivity of the liquid is affected. This certainly will be the case when treating the liquid with many pulses over a long period—the conductivity of the liquid may increase, and the conductivity of the substrate can then feed back to the characteristics of the plasma jet [46]. Certainly, there may be in-liquid transport driven by penetrating electric fields that might have biological outcomes, but this does not directly affect the electric fields delivered to the cells. It is not unambiguously clear that an increase in the conductivity of the liquid alone, as may occur with multi-pulse treatment, is a good scaling parameter to characterize delivery of electric fields to the cells. At one extreme, saline solutions are often used in studies of plasmas with cells. If sufficiently conductive and electrically grounded, the saline solution might shield the underlying cells from the electric fields produced by the plasma jet. However, if the saline solution is electrically floating, there could still likely be significant delivery of electric fields to the underlying cells.

Acknowledgments

This work was supported by the Department of Energy Office of Fusion Energy Science (DE-SC0001319) and the National Science Foundation (CHE-1124724).

References

- [1] Graves D B 2012 The emerging role of reactive oxygen and nitrogen species in redox biology and some implications for plasma applications to medicine and biology *J. Phys. D: Appl. Phys.* **45** 26
- [2] Laroussi M, Alexeff I and Kang W 2000 Biological decontamination by non-thermal plasmas *IEEE Trans. Plasma Sci.* **28** 184

- [3] Laroussi M, Kong M, Morfill G and Stolz W 2012 *Plasma Medicine: Applications of Low-Temperature Gas Plasmas in Medicine and Biology* (Cambridge: Cambridge University Press) pp 156–74
- [4] Isbary G et al 2013 Cold atmospheric argon plasma treatment may accelerate wound healing in chronic wounds: Results of an open retrospective randomized controlled study in vivo *Clin. Plasma Med.* **1** 25
- [5] Keidar M, Shashurin A, Volotskova O, Stepp M, Srinivasan P, Sandler A and Trink B 2013 Cold atmospheric plasma in cancer therapy *Phys. Plasmas* **20** 057101
- [6] Judé F, Fongia C, Ducommun B, Yousfi M, Lobjois V and Merbahi N 2016 Short and long time effects of low temperature plasma activated media on 3D multicellular tumor spheroids *Sci. Rep.* **6** 21421
- [7] Yan X, Xiong Z, Zou F, Zhou S, Lu X, Yang G, He G and Ostrikov K 2012 Plasma-induced death of HepG2 cancer cells: intracellular effects of reactive species *Plasma Process. Polym.* **9** 59
- [8] Pei X, Lu X, Liu J, Yang Y, Ostrikov K, Chu P K and Pan Y 2012 Inactivation of a 25.5 μm *Enterococcus faecalis* biofilm by a room-temperature, battery-operated, handheld air plasma jet *J. Phys. D: Appl. Phys.* **45** 165205
- [9] Winter J, Brandenburg R and Weltmann K-D 2015 Atmospheric pressure plasma jets: an overview of devices and new directions *Plasma Sources Sci. Technol.* **24** 064001
- [10] Reuter S and Sousa J S, Stancu G D and Hubertus van Helden J-P 2015 Review on VUV to MIR absorption spectroscopy of atmospheric pressure plasma jets *Plasma Source Sci. Technol.* **24** 054001
- [11] Lu X, Naidis G V, Laroussi M and Ostrikov K 2014 Guided ionization waves: theory and experiments *Phys. Rep.* **540** 123
- [12] Walsh J L, Iza F, Janson N B, Law V J and Kong M G 2010 Three distinct modes in a cold atmospheric pressure plasma jet *J. Phys. D: Appl. Phys.* **43** 075201
- [13] Sretenović G B, Krstić I B, Kovačević V V, Obradović B M and Kuraica M M 2011 Spectroscopic measurement of electric field in atmospheric-pressure plasma jet operating in bullet mode *Appl. Phys. Lett.* **99** 161502
- [14] Ghasemi M, Olszewski P, Bradley J W and Walsh J L 2013 Interaction of multiple plasma plumes in an atmospheric pressure plasma jet array *J. Phys. D: Appl. Phys.* **46** 052001
- [15] Maletić D, Puač N, Selaković N, Lazović S, Malović G, Djordjević A and Lj Petrović Z 2015 Time-resolved optical emission imaging of an atmospheric plasma jet for different electrode positions with a constant electrode gap *Plasma Sources Sci. Technol.* **24** 025006
- [16] Wild R, Gerling T, Bussiahn R, Weltmann K-D and Stollenwerk L 2014 Phase-resolved measurement of electric charge deposited by an atmospheric pressure plasma jet on a dielectric surface *J. Phys. D: Appl. Phys.* **47** 042001
- [17] Mussard M D V S, Foucher E and Rousseau A 2015 Charge and energy transferred from a plasma jet to liquid and dielectric surfaces *J. Phys. D: Appl. Phys.* **48** 424003
- [18] Kaushik N, Lee S J, Choi T G, Baik K Y, Uhm H S, Kim C H, Kaushik N K and Choi E H 2015 Non-thermal plasma with 2-deoxy-D-glucose synergistically induces cell death by targeting glycolysis in blood cancer cells *Sci. Rep.* **5** 8726
- [19] Sasaki S, Kanzaki M and Kaneko T 2014 Highly efficient and minimally invasive transfection using time-controlled irradiation of atmospheric-pressure plasma *Appl. Phys. Exp.* **7** 026202
- [20] Robert E, Darny T, Dozias S, Iseni S and Pouvesle J M 2015 New insights on the propagation of pulsed atmospheric plasma streams: from single jet to multi jet arrays *Phys. Plasmas* **22** 122007
- [21] Darny T, Robert E, Dozias S and Pouvesle J-M 2015 Electric field measurements during plasma jet operation on/in biological samples and tissues 2015 *IEEE Int. Conf. on Plasma Sciences (Belak, Antalya, Turkey)* Paper 2E-4
- [22] Weaver J C 2000 Electroporation of cells and tissues *IEEE Trans. Plasma Sci.* **28** 24
- [23] Dev S B, Rabussay D P, Widera G and Hofmann G A 2000 Medical applications of electroporation *IEEE Trans. Plasma Sci.* **28** 206
- [24] Schoenbach K H, Peterkin F E, Allen R W and Beebe S J 1997 The effect of pulsed electric fields on biological cells: experiments and applications *IEEE Trans. Plasma Sci.* **25** 284
- [25] Schoenbach K H, Katsuki S, Stark R H, Buescher E S and Beebe S J 2002 Bioelectrics—new applications for pulsed power technology *IEEE Trans. Plasma Sci.* **30** 293
- [26] Schoenbach K H, Beebe S J and Buescher E S 2001 Intracellular effect of ultrashort electrical pulses *Bioelectromagnetics* **22** 440
- [27] Beebe S J, Fox P M, Rec L J, Somers K, Stark R H and Schoenbach K H 2002 Nanosecond pulsed electric field (nsPEF) effects on cells and tissues: apoptosis induction and tumor growth inhibition *IEEE Trans. Plasma Sci.* **30** 286
- [28] Joshi R P and Schoenbach K H 2010 Bioelectric effects of intense ultrashort pulses *Crit. Rev. Biomed. Eng.* **38** 255
- [29] Vernier P T, Sun Y, Marcu L, Craft C M and Gundersen M A 2004 Nanoelectropulse-induced phosphatidylserine translocation *Biophys. J.* **86** 4040
- [30] Zerrouki A, Yousfi M, Rhallabi A, Motomura H and Jinno M 2015 Monte Carlo poration model of cell membranes for application to plasma gene transfection *Plasma Process. Polym.* at press (doi:10.1002/ppap.201500144)
- [31] Vernier P T, Sun Y, Marcu L, Craft C M and Gundersen M A 2004 Nanosecond pulsed electric fields perturb membrane phospholipids in T lymphoblasts *FEBS Lett.* **572** 103
- [32] Napotnik T B, Wu Y-H, Gundersen M A, Miklavcic D and Vernier P T 2012 Nanosecond electric pulses cause mitochondrial membrane permeabilization in jurkat cells *Bioelectromagnetics* **33** 257
- [33] Morotomi-Yano K, Akiyama H and Yano K 2011 Nanosecond pulsed electric fields activate MAPK pathways in human cells *Arch. Biochem. Biophys.* **515** 99
- [34] Alberts B, Johnson A, Lewis J, Raff M, Roberts K and Walter P 2008 *Molecular Biology of the Cell* 5th edn (New York: Taylor and Francis) pp 651–69
- [35] Garner A L, Deminksy M, Neculaes V B, Chashihin V, Knizhnik A and Potapkin B 2013 Cell membrane thermal gradients induced by electromagnetic fields *J. Appl. Phys.* **113** 214709
- [36] Norberg S A, Johnsen E and Kushner M J 2015 Formation of reactive oxygen and nitrogen species by repetitive negatively pulsed helium atmospheric pressure plasma jets propagating into humid air *Plasma Sources Sci. Technol.* **24** 035026
- [37] Tian W and Kushner M J 2014 Atmospheric pressure dielectric barrier discharges interacting with liquid *J. Phys. D: Appl. Phys.* **47** 165201
- [38] Bogey C and Bailly C 2010 Direct and large-Eddy simulation VII *Proc. 7th Int. ERCOFTAC Workshop on Direct and Large Scale Eddy Simulation VII* ed V Armenio et al (Berlin: Springer)
- [39] Rhoades R A and Bell D R 2012 *Medical Physiology: Principles for Clinical Medicine* 4th edn (Baltimore, MD: Williams & Wilkins) pp 167–77

- [40] Babaeva N Y and Kushner M J 2010 Intracellular electric fields produced by dielectric barrier discharge treatment of skin *J. Phys. D: Appl. Phys.* **43** 185206
- [41] Chizmadzhev Y A, Zarnitsin V G, Weaver J C and Potts R O 1995 Mechanism of electroinduced ionic species transport through a multilamellar lipid systems *Biophys. J.* **68** 749
- [42] Feldman Y, Ermolina I and Hayashi Y 2003 Time domain dielectric spectroscopy study of biological systems *IEEE Trans. Dielectr. Electr. Insul.* **10** 728
- [43] Ermolina I, Plevaya Y, Feldman Y, Ginzburg B and Schlesinger M 2001 Study of normal and malignant white blood cells by time domain dielectric spectroscopy *IEEE Trans. Dielectr. Electr. Insul.* **8** 253
- [44] Riès D, Dilecce G, Robert E, Ambrico P F, Dozias S and Pouvesle J-M 2014 LIF and fast imaging plasma jet characterization relevant for NTP biomedical applications *J. Phys. D: Appl. Phys.* **47** 275401
- [45] Robert E, Sarron V, Darny T, Riès D, Dozias S, Fontane J, Joly L and Pouvesle J-M 2014 Rare gas flow structuration in plasma jet experiments *Plasma Sources Sci. Technol.* **23** 012003
- [46] Hofman S, van Gils K, van der Linden S, Iseni S and Bruggeman P 2014 Time and spatial resolved optical and electrical characteristics of continuous and time modulated RF plasmas in contact with conductive and dielectric substrates *Eur. Phys. J. D* **68** 1